

# Polarimetry for Weather Surveillance Radars



Dusan S. Zrnica\* and Alexander V. Ryzhkov†

## ABSTRACT

This paper is an overview of weather radar polarimetry emphasizing surveillance applications. The following potential benefits to operations are identified: improvement of quantitative precipitation measurements, discrimination of hail from rain with possible determination of sizes, identification of precipitation in winter storms, identification of electrically active storms, and distinction of biological scatterers (birds vs insects). Success in rainfall measurements is attributed to unique properties of differential phase. Referrals to fields of various polarimetric variables illustrate the signatures associated with different phenomena. It is argued that classifying hydrometeors is a necessary step prior to proper quantification of the water substance. The promise of polarimetry to accomplish classification is illustrated with an application to a hailstorm.

## 1. Introduction

Scientific evidence accumulated over the last decade indicates that weather radar polarimetry has passed two important tests. First, as suggested by theory, polarimetric signals contain significant information about hydrometeor habits; and second, the information can be retrieved with sufficient accuracy to be useful. If it passes the cost effectiveness test, the technique should be adopted for operational applications. Although this could occur in less than 10 years, there is a large number of radar meteorologists that have not been exposed to radar polarimetry. Hence, the motivation for this paper is to present a simplified overview of the subject. Emphasized are applications to weather surveillance radars. We attempt a step in the direction well enunciated by Herzegh and Jameson (1992), who state: “While a number of significant inferences can be made from  $Z_{DR}$ , LDR, and  $Z$  observations alone, the full impact of dual-polarization

measurements will not be realized until analyses include a more complete set of simultaneous multiparameter radar observations.” To reach a broad audience, the paper touches aspects of polarimetry that are implicitly known to most radar meteorologists. Also, it provides examples of measurements obtained by the National Severe Storms Laboratory (NSSL) Cimarron polarimetric radar and speculates on future capabilities.

## 2. Polarization

At far distances from a source, the electromagnetic field is confined in a plane of polarization that is perpendicular to the propagation direction. Polarization refers to the orientation (direction) of the electric field in this plane. If its direction follows an ellipse, the field is polarized; if the ellipse changes shape and/or orientation in time, it is partially polarized; otherwise, it is not polarized. A special case is a linear polarization for which the field vector lies on a line. In nature, partially polarized and unpolarized radiation are ubiquitous; polarized radiation is an exception. For example, radiation from stars and cosmic background has no preferential polarization. But transient radiation from a well-defined cloud-to-ground lightning stroke is vertically polarized at locations on the earth’s surface not too far from the discharge. Also, forward-scattered sun

\*National Severe Storms Laboratory, Norman, Oklahoma.

†Cooperative Institute for Mesoscale Meteorological Studies, University of Oklahoma, Norman, Oklahoma.

Corresponding author address: Dr. Dusan S. Zrnica, Doppler Radar and Remote Sensing Branch, National Severe Storms Laboratory, 1313 Halley Circle, Norman, OK 73069.

E-mail: dusan.zrnica@noaa.gov

In final form 9 October 1998

radiation by cloud droplets at scattering angles of  $90^\circ$  is linearly polarized. Solar or other radiation reflected from earth's surface is partially polarized.

Anthropogenic radiation is almost always polarized. Thus, signals for radio, television, and other communications are polarized, and so are radar waves. Therefore, polarization was a part of radar meteorology from the very beginning. It happens that in the early days there were very few deliberate attempts to utilize the polarimetric information.

Models and computations were usually concerned with scatterers for which polarimetric dependence of the signal was nonexistent. For example, raindrops and hailstones were modeled as spheres (Battan 1973) so that the dependencies on the vertical or horizontal polarization were null. Yet measurements made with differently polarized radars could not produce the same result because the drops' backscattering cross sections (and, therefore, reflectivity) depend on polarization (Seliga and Bringi 1976). A drop's horizontal dimension exceeds its vertical dimension, and therefore (for drops small compared to wavelength) the cross section is larger at horizontal polarizations. At least some of the variability in measured relations between the reflectivity factor  $Z$  and rain rate  $R$  can be attributed to differences in polarization (Zrnic and Balakrishnan 1990). That is, for the same rain rate, the reflectivity factor for horizontal polarization  $Z_h$  is larger than the one for vertical  $Z_v$ .

#### a. Polarization basis

To fully capitalize on polarimetry, it is necessary to probe the hydrometeor medium with two orthogonal polarizations. Thus, polarization diversity implies a capability to rapidly measure echo characteristics at two orthogonal polarizations. This can be achieved either by changing polarization from pulse to pulse, by transmitting one and simultaneously receiving two polarizations, or both. Circular and linear polarizations have been used on weather surveillance radars. This article deals exclusively with linear polarizations whereby the orthogonal fields are designated as vertical and horizontal; at low elevation angles, these two directions almost coincide with the local horizontal and vertical direction at the radar resolution volume. A review of polarimetric radar technology, including linear and other bases, is presented by Bringi and Hendry (1990).

Horizontally polarized fields induce strong electric field responses in the same direction within the scatterer and considerably weaker responses in the

orthogonal direction. Analogous but opposite interaction applies to vertically polarized fields. These two orthogonal fields complement each other in that they can probe a hydrometeor along two perpendicular axes. Thus, differences in hydrometeor characteristics along these two axes produce corresponding responses in the interacting fields.

There are two ways in which scatterers (hydrometeors) affect polarimetric measurements. One is the backscatter (intrinsic) effect by those located within the radar resolution volume; the other is the propagation effect by those between the radar and its resolution volume. The two are often coupled and should be sorted out for identifying the type of hydrometeors in either locale. The vertical–horizontal polarization basis is well suited for surveillance radars because the electric fields are aligned with the principal axis of several hydrometeor types. This maximizes the contrasts between scattering properties of vertically and horizontally polarized waves.

#### b. Intrinsic polarimetric variables

In the linear polarimetric basis, there are six backscatter variables that can carry meaningful information (i.e., see Doviak and Zrnic 1993). These are

- 1) the reflectivity factor for horizontal polarization  $Z_h$ ;
- 2) the ratio of reflected power at horizontal–vertical polarization  $P_{hh}/P_{vv}$  called differential reflectivity  $Z_{DR}$ ;
- 3) the ratio of cross-polar power (obtained by transmitting horizontal and receiving vertical polarization) to copolar power  $P_{vh}/P_{hh}$  called linear depolarization ratio LDR;
- 4) the correlation coefficient between copolar horizontally and vertically polarized echo signals  $\rho_{hv} e^{i\delta}$ ; and
- 5) two complex correlations between the cross-polar and copolar echoes  $E(V_{hh}^* V_{hv})$  and  $E(V_{vv} V_{vh}^*)$ .

Here, the indexes on powers and voltages tell the polarization of backscattered and incident fields, except the indexes on the magnitude of the correlation coefficient  $\rho_{hv}$  specify both fields. The phase  $\delta$  of the correlation coefficient is the backscatter differential phase; it is the difference in phase between the horizontally and vertically polarized fields caused by backscattering. The nine quantities (complex quantities count as two real quantities) compose a complete set of intrinsic backscatter variables for the linear polarization basis. Of these, the correlations in 5) have not

been sufficiently explored, although they contain direct information about the mean canting angle. Henceforth, there will be no further discussion of these variables, and the first three, plus  $\rho_{hv}$  and  $\delta$ , are considered to be fundamental. Suitable combinations of these generate any other variable (e.g., from  $Z_h$  and  $Z_{DR}$ , one can obtain  $Z_v$ ).

### c. Propagation

Propagation effects that influence polarimetric measurements are

- 1) attenuation of the horizontal component,
- 2) attenuation of the vertical component,
- 3) depolarization, and
- 4) differential phase shift  $\Phi_{DP}$ .

The difference in attenuations between the horizontally and vertically polarized waves (i.e., differential attenuation) is caused by preferentially oriented hydrometeors. Differential attenuation is difficult to measure, and it can adversely affect the differential reflectivity. Depolarization is also hard to estimate, but the differential phase is a readily measured and useful parameter. In rain, the horizontally polarized waves experience larger phase shifts (lags) and propagate slower than the vertically polarized waves because raindrops are oblate and have a preferential orientation. Specific differential phase  $K_{DP}$  is a range derivative of the differential phase and can be a good indicator of liquid water and rain rate along the propagation path (Sachidananda and Zrnica 1986, 1987). Relations between these two quantities and  $K_{DP}$  with no reference whatsoever to other radar variables have been developed (Doviak and Zrnica 1993), but inclusion of additional variables (e.g.,  $Z_{DR}$ ) is thought to improve rainfall estimates (Ryzhkov and Zrnica 1995b).

To the five intrinsic polarimetric variables we add the specific differential phase to form a set of six fundamental variables. Other variables that are incorporated in some of the six can also be designated as fundamental. The present choice has practical motivation. All but one variable ( $Z$ ) are independent of the absolute receiver or transmitter calibration, and only

two variables ( $Z$  and  $K_{DP}$ ) depend on the number density of hydrometeors (Table 1). Thus, properties other than the number density are contained in four of the variables. Sometimes these properties are interdependent, so that the fundamental variables are not always independent.

### d. Wavelength

The probing wavelength can have a significant effect on the polarimetric variables. For oblate spheroids with small sizes compared to the radar wavelength and that have the dielectric constant of water, the gradual changes in size, axis ratio, and dielectric constant produce gradual changes in the polarimetric variables. But as the size increases, changes in hydrometeor properties create nonmonotonic variations in the polarimetric variables. The backscatter differential phase can be a good indicator of a size larger than about a tenth of a wavelength because at that size, it exhibits an abrupt increase (Aydin and Giridhar 1992). At smaller sizes, the backscatter differential phase decreases to zero. The transition is at 10, 5.5, and 3.5 mm for the wavelengths of 10, 5, and 3 cm, respectively.

Clearly,  $\delta$  at the 10-cm wavelength is insensitive to changes in raindrops' sizes (because drops are smaller than 10 mm), whereas at 5 and 3 cm it could be adversely affected by the drops in the range from 3 to 6 mm. Therefore, at the 10-cm wavelength, the rain-rate measurement  $R(K_{DP})$  should be more robust than at the two shorter wavelengths. For the same rain rate, however, the specific differential phase is inversely proportional to wavelength. Hence, the phase shifts at

TABLE 1. Attributes of polarimetric variables (for 5- and 10-cm wavelengths).

Attribute Variable	Independent of absolute radar	Immune to propagation effects calibration	Immune to noise bias	Used for quantitative estimation	Independent of concen- tration
$Z_h$	no	no	no	yes	no
$Z_{DR}$	yes	no	no	yes	yes
$K_{DP}$	yes	yes	yes	yes	no
$\rho_{hv}$	yes	yes	no	no	yes
$\delta$	yes	no	yes	no	yes
LDR	yes	no	no	no	yes

shorter wavelengths might be measured with lower relative errors, and that could result in better rain-rate estimates. Also, detection of mixed-phase hydrometeors might be enhanced at the 3- and 5-cm wavelengths because mixed phase is often composed of wet aggregates 5–10 mm in size, which would increase polarimetric contrasts in LDR,  $Z_{DR}$ , or  $\rho_{hv}$ .

### 3. Polarimetric variables and hydrometeor properties

Hydrometeor properties that determine the values of polarimetric variables are *number density, dielectric constant, shape, size, and orientation*. For the same properties exclusive of the dielectric constant, liquid (or liquid coated) hydrometeors have the strongest polarimetric signatures. Random orientation and irregular shape enhance some variables (LDR,  $\rho_{hv}$ ) but diminish others ( $Z_{DR}$ ,  $K_{DP}$ ). Although snow particles have a ragged shape, those growing into low-density aggregates quickly lose their polarimetric characteristics. The interplay of the properties crucially influences the polarimetric variables.

In rain,  $Z_{DR}$  is positive and related to the axis ratio of drops (Jameson 1983); it is proportional to the median diameter raised to a power of about 1.6 (Seliga et al. 1986). In clouds composed of horizontally aligned ice crystals,  $Z_{DR}$  is slightly positive. In hail,  $Z_{DR}$  can be slightly positive, zero, or negative depending if the hail is horizontally, randomly, or vertically oriented.

The correlation coefficient is high for hydrometeors that are oriented and smooth or small compared to wavelength. Thus, in rain and snow, the values are  $< 0.95$ . Tumbling hail and wet snow aggregates reduce the correlation to below 0.9.

Specific differential phase is almost linearly related to rain rate (Sachidananda and Zrnich 1987). Because it is not affected by the presence of randomly oriented scatterers, it can isolate the rain amount in the mixture with hail (Balakrishnan and Zrnich 1990; Aydin et al. 1995).

Some polarimetric variables can be affected by propagation effects, calibrations of the transmitter and receiver, and noise. Furthermore, some are suited for quantitative estimation of precipitation parameters. For comparison, a summary of attributes is provided in Table 1. Independence of transmitter–receiver calibrations is a definitive advantage and so is immunity to propagation effects and noise bias. Although nei-

ther LDR nor  $\rho_{hv}$  has provided quantitative estimates of precipitation parameters (column 5 in Table 1), these variables have ample potential for other applications. For example, both variables can indicate the presence of mixed-phase precipitation, which is very important in winter storms. Last, variables that are independent of concentration can reveal a property that is otherwise hidden (e.g., measure of axial ratio, roughness of shape); nonetheless, concentration is needed for determining bulk amounts. Therefore, the yes/no qualifiers in the last column are not associated with a particular advantage; rather, they serve only to describe the attribute.

Indications are that polarimetry has the potential to

- improve quantitative precipitation estimation;
- discriminate hail from rain and possibly gauge hail size;
- identify precipitation type in winter storms (dry/wet snow, sleet, rain);
- identify electrically active storms;
- identify biological scatterers (birds, insects) and their effects on wind measurements; and
- identify the presence of chaff and its effects on precipitation measurements.

These claims have been demonstrated by a variety of experiments. Still, much more research is needed to determine the detection probabilities, errors in measurements, and false alarm rates.

Two additional promising capabilities are being investigated, and it is unknown to what extent they might hold true. These are to

- provide initial conditions and constraints to numerical models for short term forecasts, and
- identify aircraft icing conditions.

### 4. Applications

For operational purposes, the reflectivity field is currently the primary indicator of hail or heavy rainfall. Accurate warning about these events is important to initiate evasive actions appropriate for each. Because inferences from the reflectivity factor are indirect and require analysis of storm structure and its environment, they are less reliable than those possible from the polarimetric variables, which involve direct measurements. A succinct review based on achievements in the 1980s with vivid illustrations of the LDR,

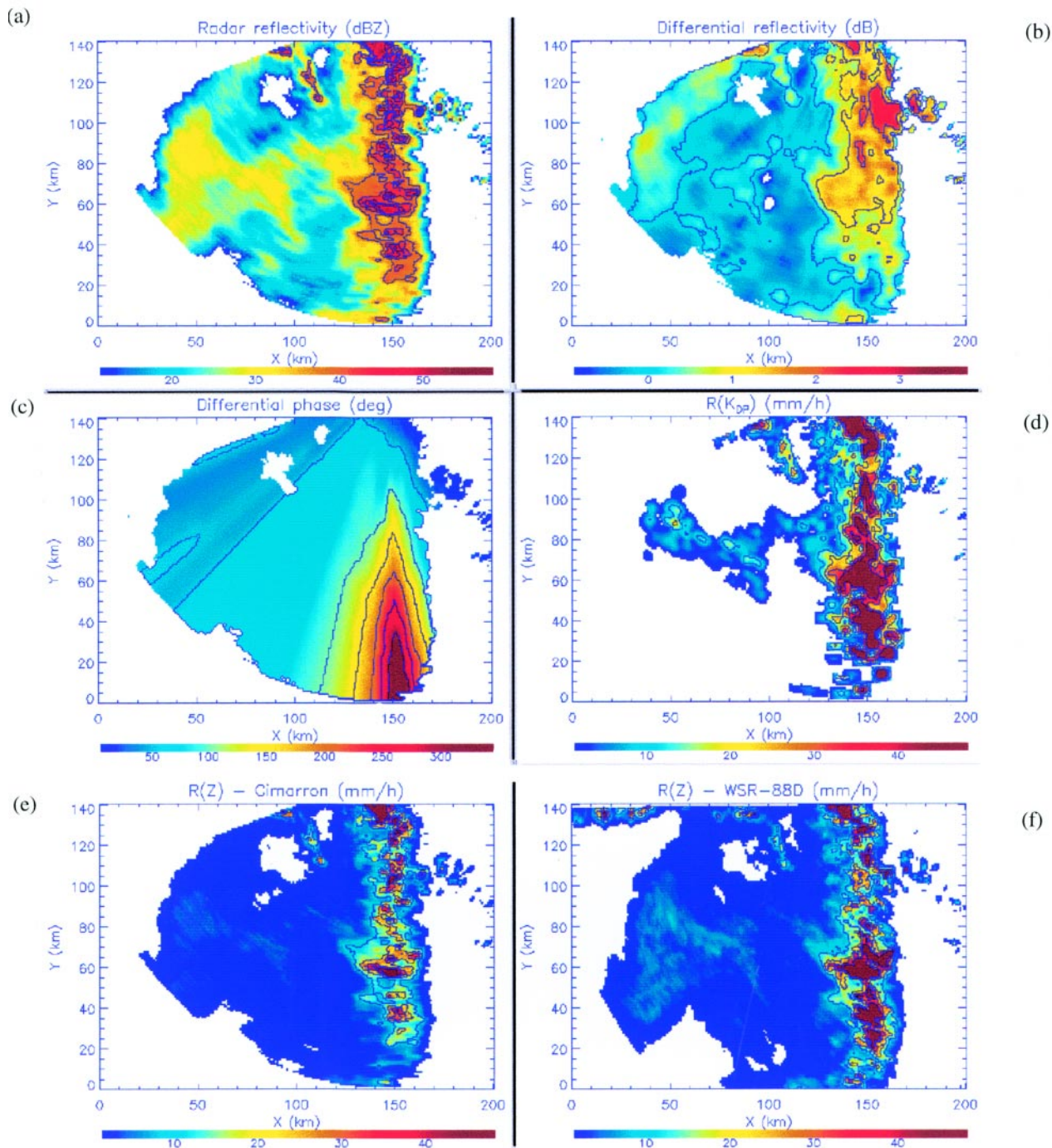


FIG. 1. (a) Reflectivity factor at the elevation of  $0.5^\circ$  for a squall line of 9 June 1993 in Oklahoma. No correction for attenuation has been applied, and the radar is located at  $X = 140$  km,  $Y = 160$  km. Color bar indicates the values in dBZ units. (b) Differential reflectivity, dB units are indicated by the color bar. (c) Differential phase, degrees are indicated by the color bar. (d) Field of rain rate  $R(K_{DP})$  obtained from the specific differential phase ( $\text{mm h}^{-1}$ ). (e) Field of rain rate obtained using  $Z$  in the  $R(Z)$  relation; data are from the polarimetric radar, that is,  $Z$  in (a). (f) Field of rain rate obtained using  $Z$  in the  $R(Z)$  relation; data are from the WSR-88D radar. In this and the rest of the figures, contour levels coincide with the numerical numbers under the color bars.

$Z_{DR}$ , and  $Z$  fields in storms and stratiform precipitation is presented by Herzegh and Jameson (1992), who conclude that a simple examination of these fields can

reveal key characteristics of the precipitation type. They point out that  $Z_{DR}$  can provide the location of liquid precipitation above the  $0^\circ$  isotherm in addition to

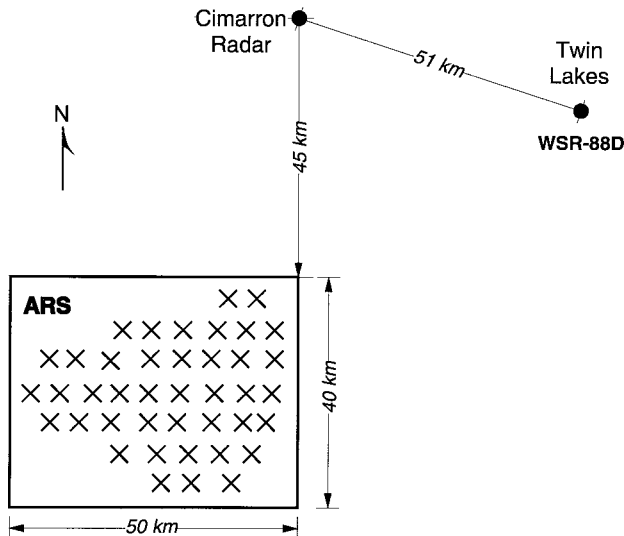


FIG. 2. Location of the polarimetric radar, the WSR-88D radar, and the Little Washita rain gauge network.

its application in rainfall estimation and surface hail detection algorithms. It is now accepted that heavy rainfall, even in the presence of hail, can be well estimated using  $K_{DP}$  (Aydin et al. 1995; Balakrishnan and Zrnica 1990), whereas combined use of  $Z$  and  $Z_{DR}$  is suitable for hail identification. Determination of hail size might be possible, and much work remains to establish the best procedures.

This section deals with the potential of polarimetric variables for measurements and identification of meteorological scatterers. Various fields of polarimetric variables are presented and related to their physical causes to illustrate several of the potentials listed in the previous section. Also included are examples of discrimination between meteorological and nonmeteorological scatterers.

#### a. Measurements of rain

Advantages of rainfall estimation from  $K_{DP}$  as opposed to  $Z$  are (Zrnica and Ryzhkov 1996) 1) it is independent of receiver and transmitter calibrations, 2) it is not affected by attenuation, 3) it is less affected by beam blockage, 4) it is not biased by ground clutter cancelers, 5) it is less sensitive to variations in distribution of drops, 6) it is little biased by the presence of hail, and 7) it can be used to detect anomalous propagation. Examples of some advantages follow.

On 9 June 1993, a squall line passed over the NSSL Cimarron radar, and polarimetric data from this event were recorded. The line produced heavy rain and, at the time of the analysis, was oriented north-south,

extending over the radar site (located at  $x = 140$  km and  $y = 150$  km in Fig. 1a, outside of the top frame). This event was examined closely to explore the utility of polarization radar techniques for rainfall monitoring (Ryzhkov and Zrnica 1995a). A surprise finding was an unexpectedly large attenuation (over 10 dB beyond 120 km) for the 10-cm wavelength, leading to large errors in conventional rainfall estimates, as will be demonstrated shortly. Furthermore, differential attenuation of 3–4 dB affected the  $Z_{DR}$  at far ranges, as can be seen by the step-like decrease of the  $Z_{DR}$  with range (Fig. 1b). The total differential phase signature (Fig. 1c) clearly demonstrates the increase caused by heavy precipitation. Rain, possibly drops with ice cores, and small, horizontally elongated hail were along the beam path in this example.

In Fig. 1d the rain rate  $R(K_{DP})$  is obtained using the specific differential phase. To reduce the effects of statistical errors, we have adapted the polarimetric rainfall estimator  $R = 40.6 K_{DP}^{0.866}$  from Sachidananda and Zrnica (1987) as follows. We separate light from heavy rainfall with a 40-dBZ reflectivity threshold. In areas of light rain, we use an averaging scale (~10 km) for differential phase data three times longer than in areas of heavier rainfall.

The rain-rate field in Fig. 1e is obtained by applying the Marshall–Palmer relation  $Z = 200R^{1.6}$  to the reflectivity field of Fig. 1a. At about the time the data in Figs. 2a–e were collected, a WSR-88D radar was surveying the same storm. Because the WSR-88D is located at  $x = 190$  km and  $y = 140$  km (Fig. 2; see location grid, Fig. 1), its radiation did not experience as much attenuation in the squall line as did the radiation from the polarimetric radar. This is confirmed by the field of rain rate in Fig. 1f, which agrees with the  $R(K_{DP})$  field (Fig. 1d). Clearly, the reflectivity factor values of the polarimetric radar are attenuated, leading to underestimation of rainfall (Fig. 1e). The large attenuation is attributed to small hail and/or large drops with ice cores (Ryzhkov and Zrnica 1995a).

Differential phase allows rainfall estimation in regions where the beam is partially blocked. This is important because lowering elevations minimizes 1) the influence of precipitation evolution with height, 2) the horizontal drift of hydrometeors as they fall from the resolution volume to the ground, and 3) contamination by the bright band (the enhanced reflectivity region at the height where ice hydrometeors are melting). For the Cimarron radar, the beam is blocked to 0.2° by a ridge that extends from southeast to west of the radar. This is also where a network

of 42 rain gauges is located (Fig. 2), which prompted us to compare rainfall accumulations by the gauges, the  $R(Z)$  method, and the polarimetric  $R(K_{DP})$  method at the  $0^\circ$  elevation.

The two-hour rain accumulation field obtained from  $R(K_{DP})$  has significantly larger values than the field obtained from  $R(Z)$ , and it agrees much better with the gauges (Fig. 3). The mean rainfall rate  $\langle R \rangle$  (defined as accumulations divided by area and time) areas follow: for the gauges,  $3.9 \text{ mm h}^{-1}$ ; and for  $R(Z)$ ,  $1.8 \text{ mm h}^{-1}$ . The underestimate is mostly due to beam blockage; over 70% of the beam is blocked, which amounts to about 6.4 dB of power loss (Zrníc and Ryzhkov 1996).

In 15 Oklahoma rain storm cases,  $R(K_{DP})$  outperformed the  $R(Z)$  estimates both in terms of bias and standard errors of the estimates (Ryzhkov and Zrníc 1996). The fractional standard error for the  $R(K_{DP})$  algorithm was 14%, whereas it was 34% for the  $R(Z)$  algorithm. Corresponding biases were about  $-12\%$  and  $-28\%$ . This favorable performance of the  $R(K_{DP})$  estimator is likely caused by its lower sensitivity to drop size distribution variations compared to the  $R(Z)$  estimator. Nonetheless,  $R(K_{DP})$  is affected by the median drop size, its oblateness, and to some extent by the presence of large drops. Jameson (1991) and Ryzhkov and Zrníc (1995b) combined  $K_{DP}$  and  $Z_{DR}$  to obtain a rain rate almost independent of the median drop shape. Statistical analyses of data from different climate regions are required to evaluate this combined use of the two polarimetric variables.

Anomalous propagation (AP) affects precipitation measurements in that it causes ground echoes at far distances from the radar. Two facets of the problem need to be addressed. AP-induced ground clutter should be recognized, and rainfall should be estimated in the area contaminated with the clutter. Somewhat fortuitously, polarimetry addresses both aspects.

It has been experimentally determined that the  $\rho_{hv}$  of ground clutter is relatively low (Ryzhkov et al.

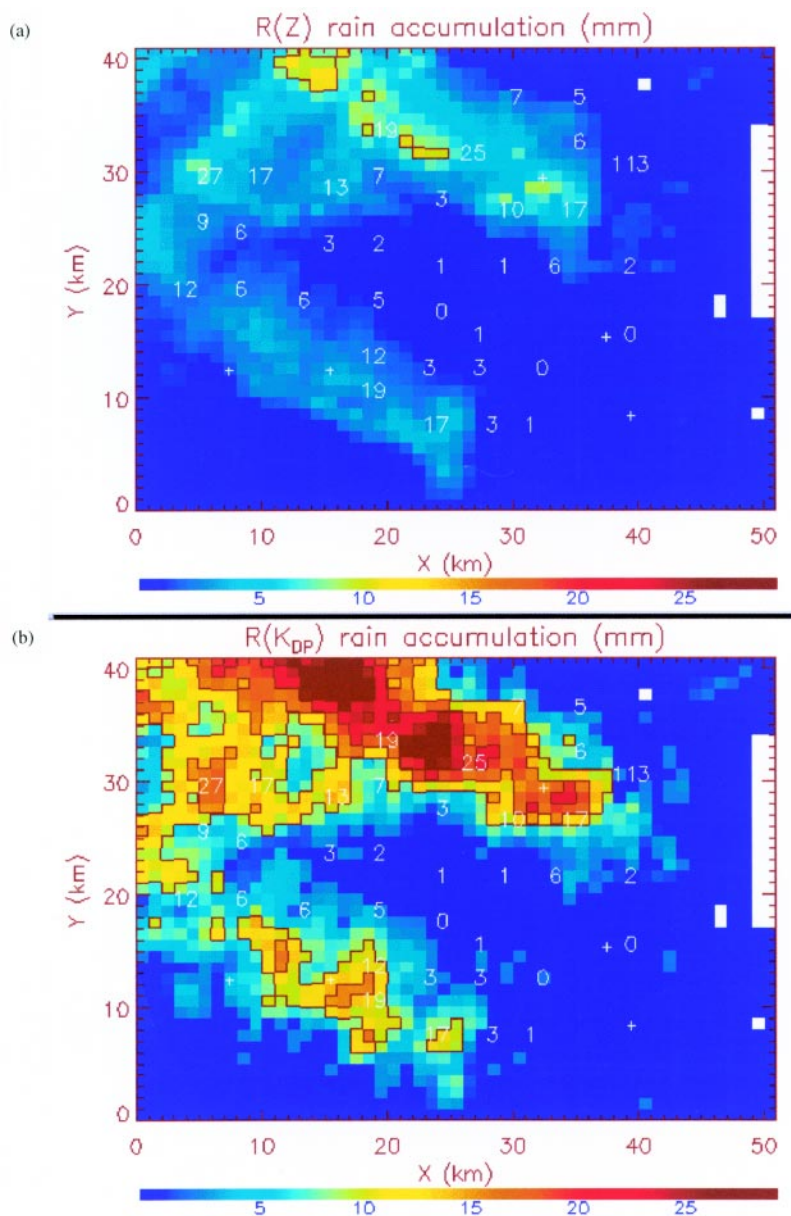


FIG. 3. Rain accumulations (mm) computed from (a) the Marshall–Palmer  $R(Z)$  relation and (b) the  $R(K_{DP})$  relation, from data at the  $0^\circ$  elevation. The white numbers indicate rain depths at gauge locations.

1994). Thus, a threshold applied to  $\rho_{hv}$  could separate precipitation from ground clutter. A value of 0.7 works well on the data from the Cimarron polarimetric radar, as can be seen in Fig. 4. The precipitation cells in Fig. 4a are south of the radar and advect to the southeast. Immediately behind the cells is a stratiform rain region, and west through northeast is where ground clutter appears. Application of the 0.7 threshold eliminates most of the contaminated reflectivity data (Fig. 4b). This we have verified by comparing to

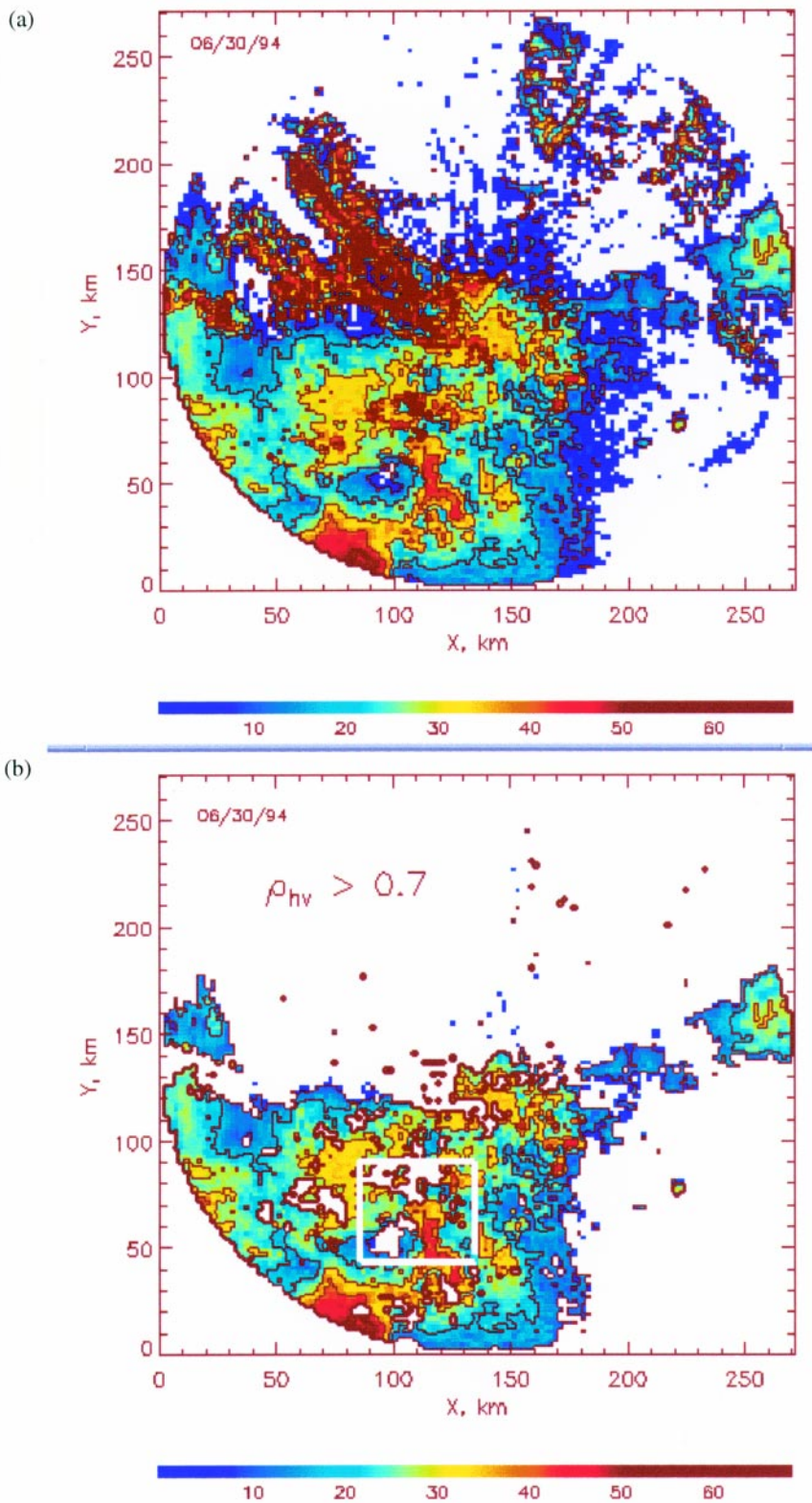


FIG. 4. The reflectivity factor  $Z$  field at the elevation of  $0.5^\circ$  for the storm of 30 June 1994; (a) all  $Z$ s are displayed; (b)  $Z$ s with  $\rho_{hv} < 0.7$  are displayed. The white rectangle encloses the gauge network. Contours are drawn every 10 dB starting at 10 dBZ.

gauges (in the area enclosed by the white rectangle) and by examining the scan at the next elevation angle.

Use of the specific differential phase to estimate rainfall automatically excludes areas contaminated with the ground clutter. This is because the standard deviation of the differential phase from ground clutter is very large and, therefore, does not pass a valid data test, leaving data-void segments. These gaps in data are linearly interpolated. If there is rain in the region of a data gap, it would show as an increase of differential phase at the end of the gap, so the interpolated values represent a path-averaged rainfall. Illustration of this useful feature is in Fig. 5. The granular texture of the reflectivity factor in the rain gauge area (Fig. 5a) suggests the presence of AP clutter. Comparison of the rain depth field (Fig. 5b), obtained using the  $R(Z)$  relation, with the gauges' field (Fig. 5c), reveals regions contaminated by the AP clutter. Note that the gauges' rain depth field was obtained by interpolating individual accumulations to a Cartesian grid with 1-km spacing. The rain accumulation from  $R(K_{dp})$  agrees well with the gauges, as can be seen in Fig. 5d.

#### b. Measurements in snow

A large part of the United States is frequented by snowstorms. Further, because the United States extends substantially in latitude, a single weather system can produce rainfall in the south and snowfall in the north of the country. In between, there can be mixed-phase precipitation. Often, there is a tem-

poral transition between these three types of precipitation at the same location. Remote delineation of the transition region between rain and snow is of great importance because these two precipitation types have vastly different, yet significant, social and economic impacts in the regions of occurrence. Forecasts of the expected location of rain/snow boundaries are somewhat elusive and often based on incomplete or inadequate climatological information. Knowledge of the exact location of the rain–snow boundary is also necessary to accurately determine the precipitation amounts.

Polarimetry can help identify the precipitation type, and the transition region, and has the potential to improve quantitative measurement. Recent observations in winter Oklahoma storms indicate that  $K_{DP}$  and  $Z_{DR}$  from dry snow are independent of the reflectivity factor if  $Z < 35$  dBZ (Ryzhkov and Zrníc 1998). Both are small with  $K_{DP} < 0.08$  deg km<sup>-1</sup> and  $Z_{DR} < 0.6$  dB. In convective winter storms with mixed precipitation and  $Z$  above 35 dBZ,  $Z_{DR}$  provides significant contrast between rain and snow, and a decrease in  $\rho_{hv}$  coincides with the transition region between rain and snow.

As a typical example, the  $Z$  field from the storm of 18 December 1995 (Fig. 6a) exhibits a maximum of about 45 dBZ. The radar reflectivity pattern gives no clues of a transition between snow and rain, whereas the corresponding differential reflectivity pattern is highly informative (Fig. 6b). A ridge of high  $Z_{DR}$  exceeding 2 dB clearly delineates the transition region between snow and rain. The position of the 1°C isotherm near the surface coincides with the actual snow–rain transition line. At the same location, a localized deep minimum of the correlation coefficient  $\rho_{hv}$  was also observed. The signature in the two fields is similar to the one found in the horizontal melting layer of stratiform rain and is attributed to the transformation of large snowflakes into raindrops. In this winter storm, the “bright band” is vertically elongated (Stewart 1992) and extends only for about 10 km in the horizontal direction.

Advection of this bright band is seen in temporal changes

of  $Z$ ,  $Z_{DR}$ ,  $K_{DP}$ , and  $\rho_{hv}$  (Fig. 7). The values in Fig. 7 are averages over a 10 × 10 km<sup>2</sup> area [centered on Norman at coordinates (210, 156) km in Fig. 6] of the data which were collected at 0.5° in elevation. Therefore, the corresponding height of the beam center is between 400 and 550 m above ground. The change from pure rain to rain–snow mixture occurred at time = 103 min (2140 UTC). That time is within the interval of abrupt transition in  $Z_{DR}$  (from 2.3 to 0 dB). The correlation coefficient reaches its minimum at time = 95 min, just before snow was first detected on the ground. The specific differential phase exhibits its maximum simultaneously with the  $\rho_{hv}$  minimum. At time = 133 min, very large (~2 cm) snowflakes were detected on the ground; that is the time the reflectivity reaches its maximum, whereas  $Z_{DR}$  and  $K_{DP}$  are low because the bulk density of snowflakes is very low.

Correct mapping of the reflectivity factor field from snow into snowfall amounts is more complicated than relating  $Z$  to rain, and verification of snowfall rates is very difficult. That is, perhaps, why significant attempts to develop polarimetric methods for snowfall measurements have yet to be made. Nonetheless, polarimetric potential can be demonstrated on measurements of ice water content (IWC) in clouds.

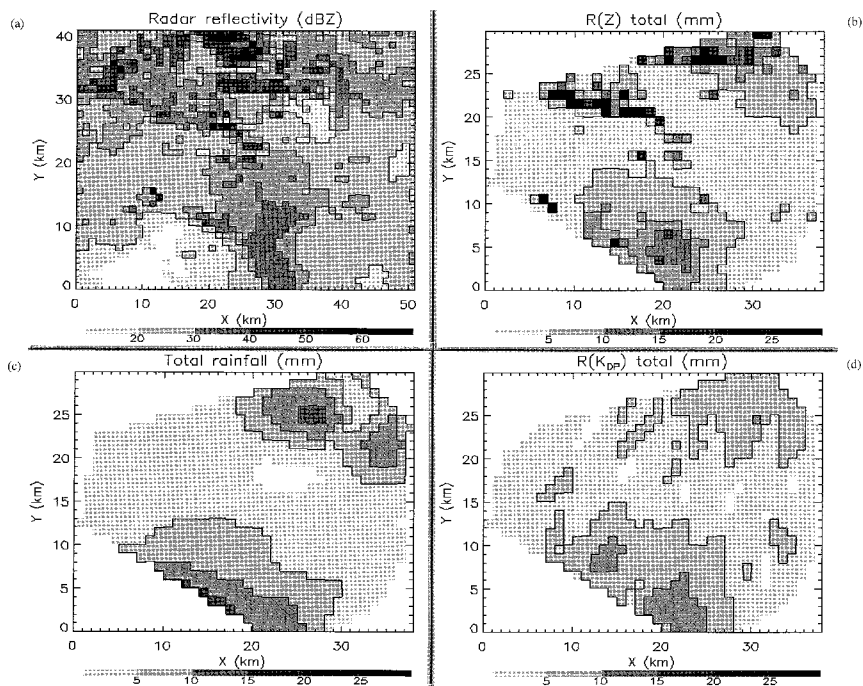
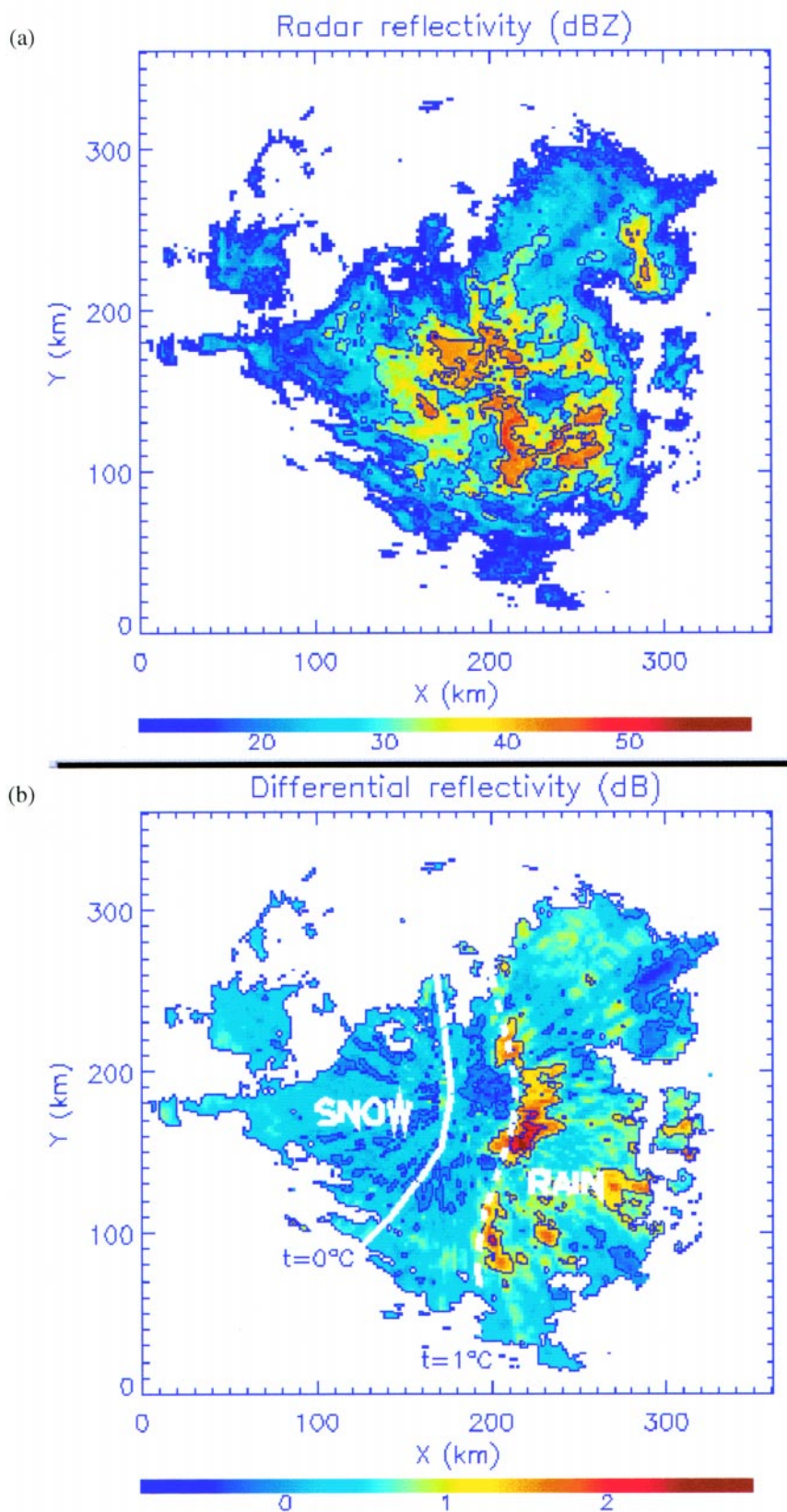


FIG. 5. (a) The reflectivity field in the area of the gauges for the same storm as in Fig. 4. (b) The rain depth field for one hour of rain obtained from the Marshall–Palmer  $R(Z)$  relation. (c) The rain depth field from the rain gauges. (d) The rain depth field from the  $R(K_{DP})$  relation.



Vivekanandan et al. (1994) derived a linear relation between  $K_{DP}$  and IWC that contains the axis ratio of hydrometeor. Ryzhkov et al. (1998) proposed the relation  $IWC = 0.29 \lambda K_{DP}$ . Crystals have well-pronounced polarimetric signatures and, thus, can be quantified using  $K_{DP}$  and  $Z_{DR}$  with the following equation (Ryzhkov et al. 1998):  $IWC = 0.044 \lambda K_{DP} / (1 - 10^{-0.1Z_{DR}})$ , where IWC is in  $g m^{-3}$ ,  $\lambda$  is the radar wavelength in cm, and  $K_{DP}$  is in  $deg km^{-1}$ . The formulas are valid for pristine and lightly to moderately aggregated crystals.

A test of the method was made for the case of 21 May 1995, during which the Cimarron polarimetric radar detected a region of high  $K_{DP}$  aloft in the trailing precipitation behind a squall line. A well-pronounced region of high specific differential phase was centered at the height of 6 km and extended about 20 km in the horizontal direction. Maximum  $K_{DP}$  in this region was about  $0.6 deg km^{-1}$ , maximum  $Z_{DR}$  was slightly above 1 dB, whereas the reflectivity factor was less than 25 dBZ.

The instrumented T-28 aircraft (South Dakota School of Mines and Technology) penetrated the region of high  $K_{DP}$  at an average altitude of 6.3 km, where the ambient air temperature was between  $-15^\circ$  and

FIG. 6. Fields of (a) reflectivity factor (in dBZ), and (b) differential reflectivity (in dB), to which the  $0^\circ$  and  $1^\circ C$  surface isotherms are superposed. Color categories at the bottom of each figure indicate the actual values of the variables; this snow storm occurred on 18 December 1995.

-16°C. From this height 2D-P probe data indicate the presence of pristine crystals and small aggregates with maximum sizes below 3 mm. Ice water content computed from the measurements on board the T-28 aircraft and the radar estimates are illustrated in Fig. 8. The polarimetric algorithm  $IWC(K_{DP}, Z_{DR})$  yields a better agreement with in situ measurements than the algorithm that uses an  $IWC(Z)$  relation (Atlas et al. 1995).

Given the accuracy of  $K_{DP}$  estimates achievable at the 10-cm wavelength, our results suggest that reasonable estimates of IWC should be possible for amounts exceeding about  $0.1 \text{ g m}^{-3}$ . To quantify lower IWCs using a similar technique, radars with shorter wavelengths are needed.

### c. Measurements in a hail storm

Soon after the introduction of linear dual polarization (LDR) to radar meteorology, the role of differential reflectivity for hail detection was recognized (Bringi et al. 1984). Numerous examples of hail signatures, consisting of high  $Z$  and near-zero  $Z_{DR}$  in the precipitation core close to the surface, have been reported. A fine example, which also contains LDR, is from a severe Denver storm of 1984 (Herzogh and Jameson 1992). The case that we present next is very similar, except it has no LDR but has  $K_{DP}$  and  $\rho_{hv}$ .

Vertical cross sections of  $Z$ ,  $Z_{DR}$ ,  $K_{DP}$ , and  $\rho_{hv}$  (Fig. 9) illustrate the additional information about hydrometeors that these variables together provide. The information is relevant for hail detection, which is discussed next, as well as identification of hydrometeors in general. The cross sections are reconstructions from conical scans.

In this case, the extent of the 55-dBZ core (Fig. 9a) suggests that the storm is producing hail. This is reinforced by the intrusion of low  $Z_{DR}$  values (Fig. 9b,  $x = 65 \text{ km}$ ,  $y = 2.5 \text{ km}$ ) below the melting level, which is marked with the gradient of  $Z_{DR}$  ( $x = 40$  to  $60 \text{ km}$ ,  $y = 3.5 \text{ km}$ ) and a decrease of  $\rho_{hv}$  (Fig. 9c,  $x = 40$  to  $60 \text{ km}$ ,  $y = 3.5 \text{ km}$ ). The intrusion of low  $Z_{DR}$  values is caused by hail that did not have enough time to melt. Closer to the ground (at the same range), the smallest hail has melted and/or larger hail has started to shed drops.

Two intrusions of  $Z_{DR}$  above the melting level indicate the presence of horizontally oriented scatterers,

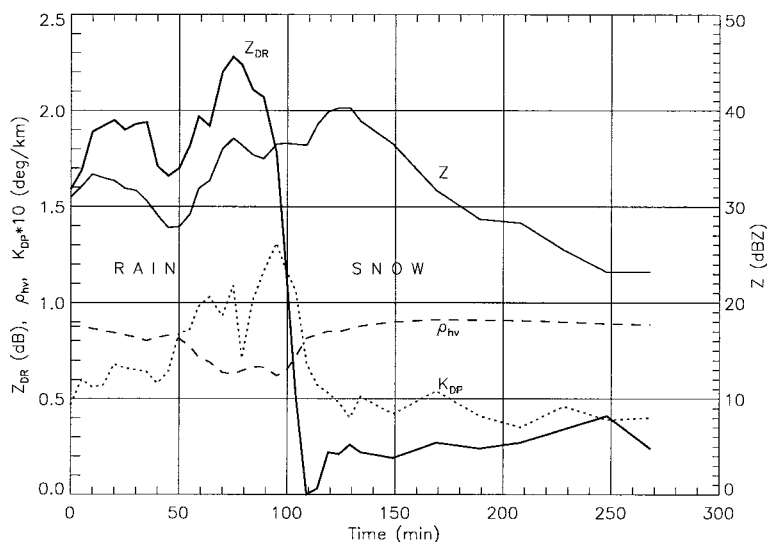


FIG. 7. Temporal dependence of  $Z$ ,  $Z_{DR}$ ,  $K_{DP}$ , and  $\rho_{hv}$  at Norman for the storm of 18 December 1995.

likely rain. Presence of the heaviest rain is implied where the specific differential phase has maximum values. These locations coincide with the reflectivity core up to about 7 km in height. Note the collocation and difference in widths of the  $Z_{DR}$  and the  $K_{DP}$  columns ( $x = 60 \text{ km}$ , Figs. 9b,c). Some of the increase in the width of the  $K_{DP}$  column could be caused by filtering in range ( $\sim 2 \text{ km}$ ). Low values of  $\rho_{hv}$  extend through the height of the reflectivity core, perhaps due to tumbling hail. Thus, concerning the core of the storm, from polarimetry, one can infer that rain mixed with hail is falling between 50 and 70 km in range, and mainly rain is falling at  $x < 50 \text{ km}$ . Furthermore, a significant

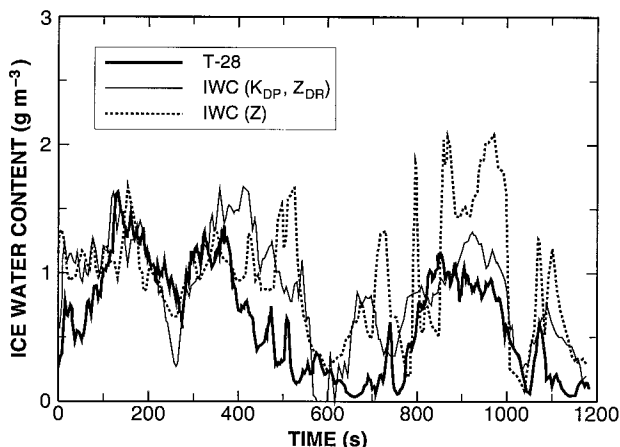


FIG. 8. Comparison of the results of in situ measurements of IWC (thick solid line) with the IWC estimates derived using  $Z$  (dashed line) and the joint  $K_{DP}$  and  $Z_{DR}$  measurements (thin solid line).

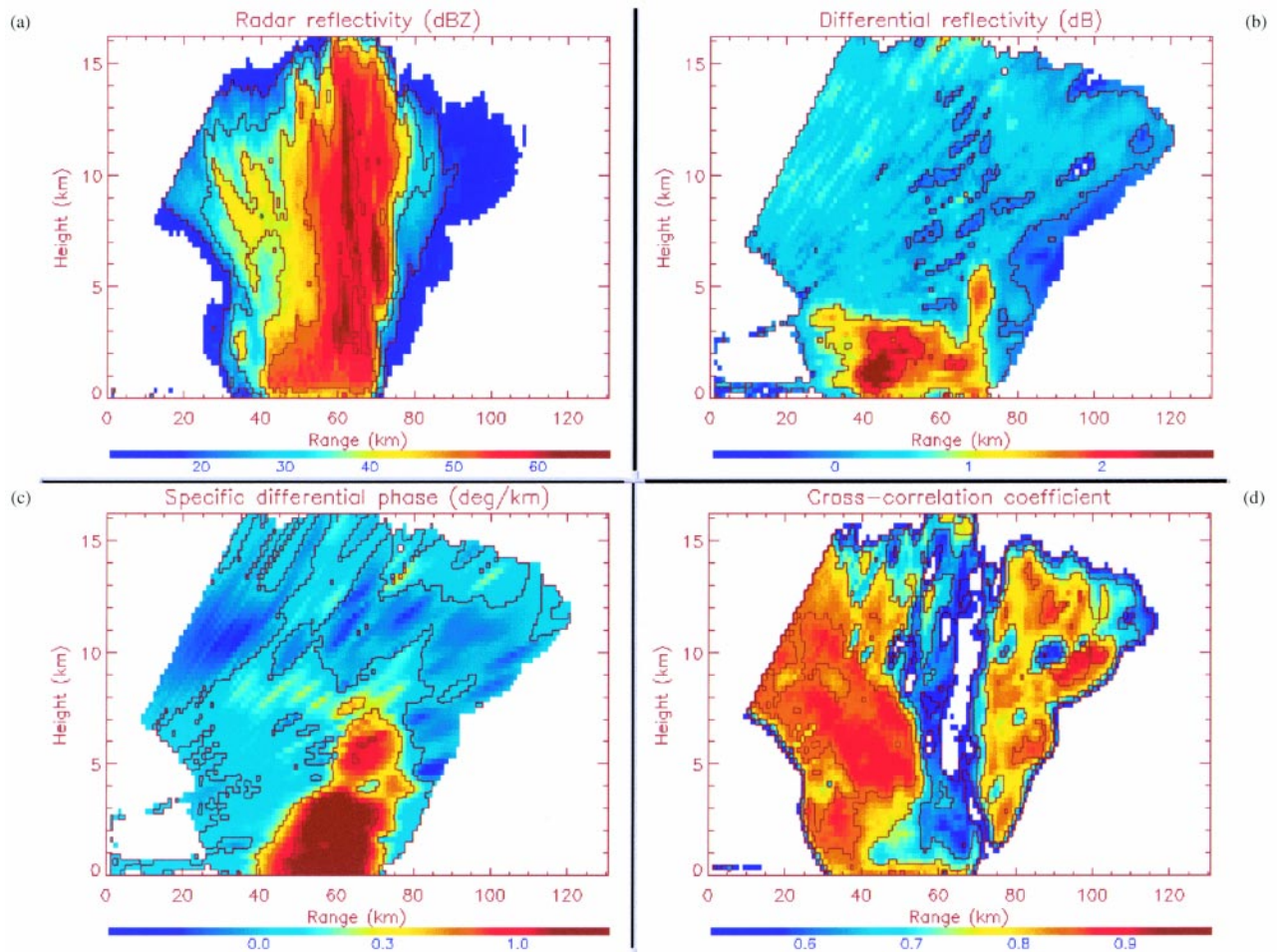


FIG. 9. Vertical cross section of (a) reflectivity factor (dBZ), (b) differential reflectivity (dB), (c) specific differential phase (deg km<sup>-1</sup>), and (d) correlation coefficient. This hail storm occurred on 6 June 1996.

amount of supercooled water is brought up above the melting level.

Above the melting level, minima of differential reflectivity are generally collocated with the core (Fig. 9b), supporting the notion that hail is aloft. In the anvil and top of the storm, the  $Z_{DR}$  is small and positive, possibly due to oriented pristine ice crystals. The specific differential phase exhibits an increasing trend as the height decreases, perhaps due to increased number concentrations. Although we have no independent verification to corroborate conclusions based on the polarimetric variables, coherency and spatial continuity of the fields boost our confidence in the interpretation.

#### d. Classification of hydrometeors

The example in Fig. 9 is well suited to demonstrate the potential of polarimetry for the classification of hydrometeors. This, we believe, is a fundamental condition

for accurate determination of precipitation amounts. First, a correct classification needs to be made, and then, appropriate semiempirical relations should be applied to each class to estimate the corresponding amounts. This is quite different from the current practice (with reflectivity in the operational world), whereby the choice is between a few relations, and the operators decide if precipitation is frozen or liquid.

We classify the observed hydrometeors in the following categories: 1) light rain ( $R > 5 \text{ mm h}^{-1}$ ), 2) moderate rain ( $5 > R > 30 \text{ mm h}^{-1}$ ), 3) heavy rain ( $R > 30 \text{ mm h}^{-1}$ ), 4) hail, 5) rain–hail mixture, 6) graupel or small hail, 7) wet snow, 6) dry snow, and 7) ice crystals.

Our automatic classification procedure (to be described shortly) has produced the fields of hydrometeors (Fig. 10) that generally agree with the human interpretation in the previous section. The hail column is determined by the  $Z$ ,  $Z_{DR}$  values, and within it, the field of rain–hail mixture is primarily influenced by

the  $Z$ ,  $K_{DP}$  pairs. We recognize that the transition between graupel and rain at 3.5 km reflects the weighting by the  $Z_{DR}$ ; however, the column of liquid water associated with the  $Z_{DR}$  intrusion above the melting zone is not identified. The rain intensity decreases away from the core, and crystals are located mainly in the anvil region. Sporadic misclassifications appear as isolated patches within continuous fields. The results presented here and elsewhere (Straka and Zrníc 1993; Straka 1996; Meischner et al. 1997) are very promising, yet much testing and comparisons with in situ measurements are required to evolve the algorithm into a useful tool. A brief description of the classification scheme follows.

For a given precipitation type, the polarimetric variables cluster in a specific region of the multidimensional space. The crux of the classification process is to separate overlapping clusters so that the probability of correct classification is high, while the probability of misclassification is low. This is a classical statistical decision theory problem that could be solved if the statistics relating the variables to the class of hydrometeors were available. Approaches based on nonlinear mapping, exemplified by neural networks, are not suitable either because there are no training sets to tune the network. A promising approach is that proposed by Straka and Zrníc (1993) and Straka (1996), which relies on fuzzy classifiers (Mendel 1995). The algorithm cannot “improve itself by learning” as neural networks do, but is simple, easy to modify, and quite intuitive.

Classification is based upon weights assigned to the various multiparameter variables. The choice of weights is founded on previous measurements, physical reasoning, modeling, etc., as alluded to in the preceding section. In our version of the algorithm, the weights  $W$  are functions of two variables at a time; one is always the reflectivity factor, and the other is one of the remaining polarimetric measurands. For example, ice hydrometeors can be separated from rain by a curve in the  $Z_{DR}$ – $Z$  plane (Aydin et al. 1986). The boundary is not perfect, and on either side, ice and liquid phase hydrometeors can coexist. At the boundary, the weighting function of ice and water are equal [ $W_i(Z, Z_{DR}) = W_w(Z, Z_{DR}) = 0.5$ ]. Toward the region of pure ice,  $W_i$  gradually increases to 1, while  $W_w$  decreases to 0. Typically, weights are non-zero for more than one hydrometeor type because several species might produce the same values of some polarimetric variables. The hydrometeor type chosen by the algorithm is the one with the highest mean score (average of weights corresponding to each polarimetric variable). Because classification of hydrometeor types based

on polarimetric variables is not always unique, the algorithm is constrained by other physical factors such as the environmental air temperature (e.g., at temperatures above freezing, dry snow usually does not exist).

#### e. Effects of lightning and electrification

Three time constants pertinent to radar observations of electric phenomena in storms can be identified. A short time constant from tens of microseconds to a few hundred milliseconds is associated with the lightning channel; to observe such fast phenomena, the antenna beam needs to be fixed for the duration of the discharge, and a thorough analysis requires spectral processing (Zrníc et al. 1982). A medium time constant of hundreds of milliseconds to a few seconds corresponds to the time it takes ice crystals to reorient after abrupt change in electric fields caused by a discharge. A longer time constant corresponds to buildup of charge and, thus, fields; these, in turn, can orient the crystals in a preferential direction.

To the authors’ knowledge, spectra of polarimetric data from the lightning channel have not been reported. But there are documented cases where lightning intersected the beam and produced a decrease of  $\rho_{hv}$  (Caylor and Chandrasekar 1996). It is highly probable that lightning occurrence produces perturbations of the backscatter polarimetric variables, which are interpreted as noise. The effects on the variables depend on the geometric configuration of lightning in the resolution volume.

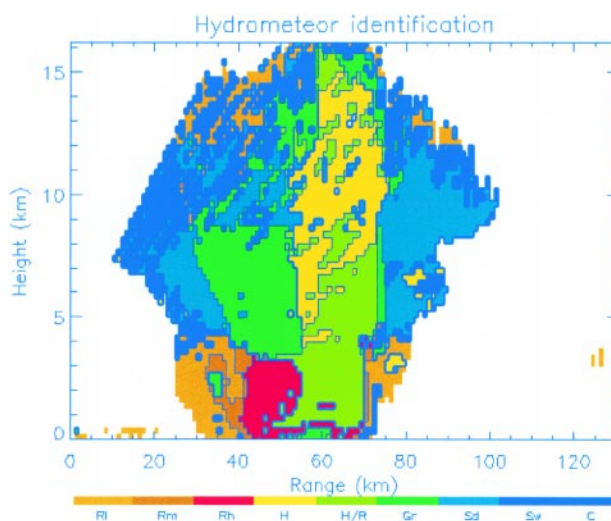


FIG. 10. Classification of precipitation whose polarimetric fields are in Fig. 9. Labels of the color bar are as follows: RI is light rain, Rm is moderate rain, Rh is heavy rain, H is hail, H/R is hail–rain mixture, Gr is graupel or small hail, Sd is dry snow, Sw is wet snow, and C is ice crystals.

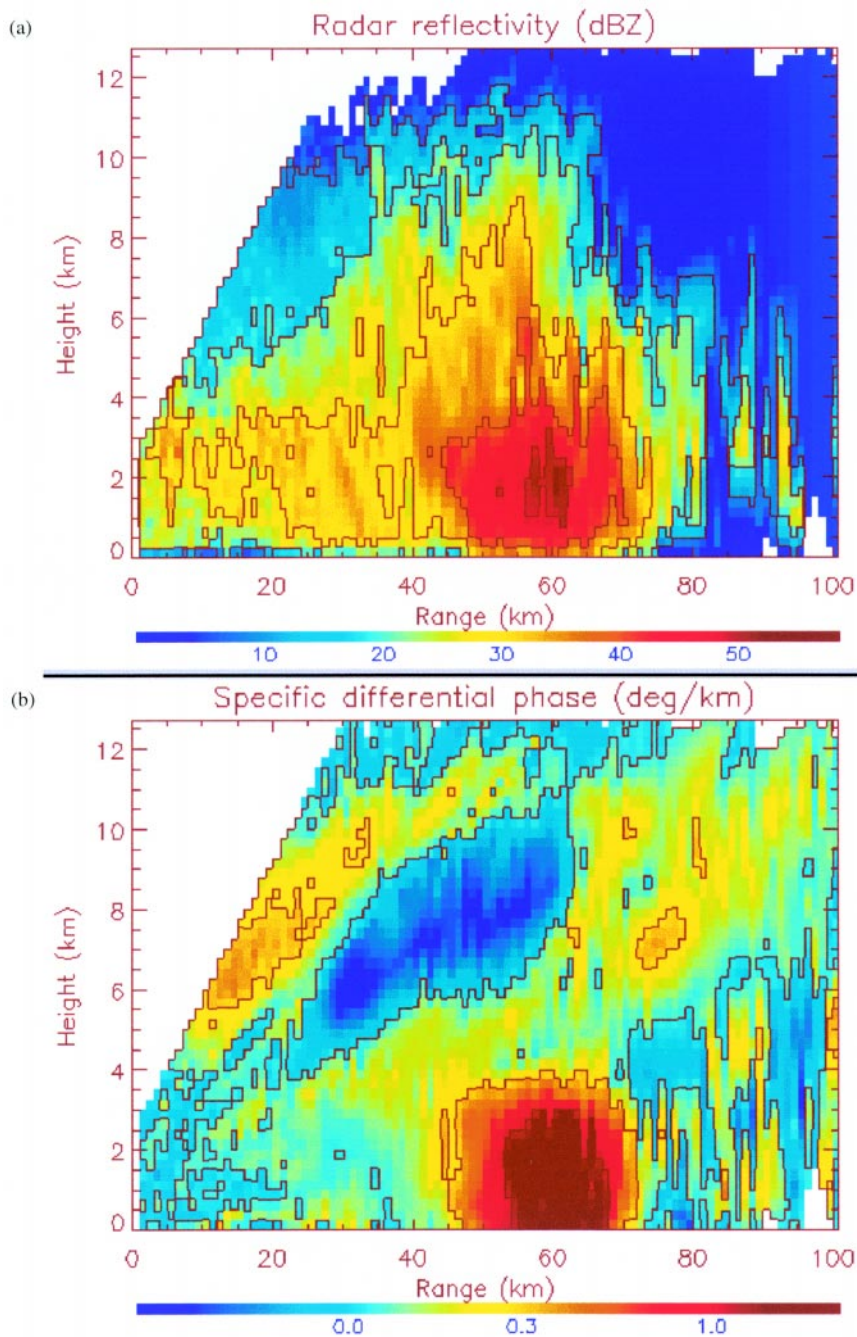


FIG. 11. Vertical cross section of (a) reflectivity factor (dBZ) and (b) specific differential phase ( $\text{deg km}^{-1}$ ). The storm occurred on 7 May 1995; the azimuth is  $104^\circ$ , and the time is 1933 UTC.

Changes in polarimetric variables corresponding to the medium and longer time constants have been observed first by communication specialists interested in propagation effects (Hendry and McCormick 1976). These were attributed to changes in orientation of ice crystals under the influence of electric fields. Recent observations with a circularly polarized radar (Metcalf 1993, 1997; Krehbiel et al. 1996) indicate that the

propagation effects dominate and that the backscatter effects are not discernible. In the linear polarization basis, the variables that respond to changes are  $K_{\text{DP}}$  and LDR. Convincing examples of negative  $K_{\text{DP}}$  fields and LDR attributed to vertically oriented ice crystals at storm tops are presented by Caylor and Chandrasekar (1996). Absence of associated signatures in the  $Z_{\text{DR}}$  fields suggests that the polarimetric signatures are caused by propagation effects and that the dominant contributors are by small (1 mm or less) oriented ice crystals.

Vertical cross sections of the reflectivity factor (Fig. 11a) and specific differential phase (Fig. 11b) through an Oklahoma convective storm illustrate regions of oriented crystals. The region of negative  $K_{\text{DP}}$  extends from 5 to 10 km in height and 20 to 60 km in range (Fig. 11b). This region is mostly above the strong reflectivity core (Fig. 11a). Its likely cause is intense electric fields that have vertically tilted numerous small ice crystals. Note that horizontally oriented crystals have created positive  $K_{\text{DP}}$  signatures adjacent to the negative one between 6 and 10 km in height. Significant positive  $K_{\text{DP}}$  between 45 and 65 km and below 4 km height is due to rain.

Evolutions of this and similar changes in  $K_{\text{DP}}$  occur at volume update times of tens of seconds. That is, the region of negative  $K_{\text{DP}}$  is generally stable, but there are changes of small-scale structure possibly due to lightning discharges between the scans. At volume update times of several minutes, the changes can be so significant that the successive fields bear no resemblance to each other. It remains to be seen if one could infer the field strength and charge amounts from similar observations.

#### f. Nonmeteorological scatterers

Some nonmeteorological scatterers, such as insects, birds, ground clutter, and chaff, present discernible signatures in the fields of polarimetric variables. A discussion with some examples follows.

##### 1) INSECTS AND BIRDS

Detection of insects and birds can have a twofold significance. For entomologists and ornithologists, there is an opportunity to identify days when insects or birds are migrating. If these biological scatterers are strong flyers, they produce a bias in Doppler wind estimates that needs to be eliminated from meteorological analysis. The  $Z_{DR}$  backscatter differential phase  $\delta$  pairs have discriminatory properties to separate small song birds from insects (Zrnica and Ryzhkov 1998), as can be seen in Fig. 12. We do not have in situ proof for the presence of either scatterer, but we rely on accepted facts that the migration of songbirds is in the fall or spring and at night, and that insects permeate the boundary layer during hot summer afternoons. The insect echoes grow with the development of the mixed layer, which is what we observed. Particularly noteworthy are azimuthal patterns of these variables for either species. Mueller and Larkin (1985) present polar plots of differential reflectivity that show maxima (about 7 dB) in azimuths where the radar is observing the broad (aligned with the wind) side of insects. We observed similar patterns of  $Z_{DR}$  with maximum values of over 10 dB (Zrnica and Ryzhkov 1998). The azimuthal variation of  $\delta$  was less than  $40^\circ$ , and the  $\rho_{hv}$  was between 0.3 and 0.5. The insect sizes barely enter the resonance scattering regime and, therefore, do not produce a noticeable azimuthal pattern of  $\delta$ . Although some contrast between insects and birds can be seen in  $Z_{DR}$  fields, it is strongest in the patterns of  $\delta$ .

The reflectivity field of migrating passerines (Fig. 13a) hints to the presence of anisotropic scatterers but by itself is somewhat deficient. The fields of differential reflectivity (Fig. 13b) and backscatter differential phase (Fig. 13c) are rich in detail, characteristic of small birds (Zrnica and Ryzhkov 1998). Notice how both  $Z_{DR}$  and  $\delta$  are symmetric with respect to the  $45^\circ$  azimuth but are not circularly symmetric. This is because the bird's head view is different from its tail view. On that October evening (2123 CST), the migration was from northeast to southwest, so it follows from Fig. 13a that the cross sections looking at the tails are considerably smaller than the ones presented by the heads' view. Also,  $Z_{DR}$  indicates a small local maxi-

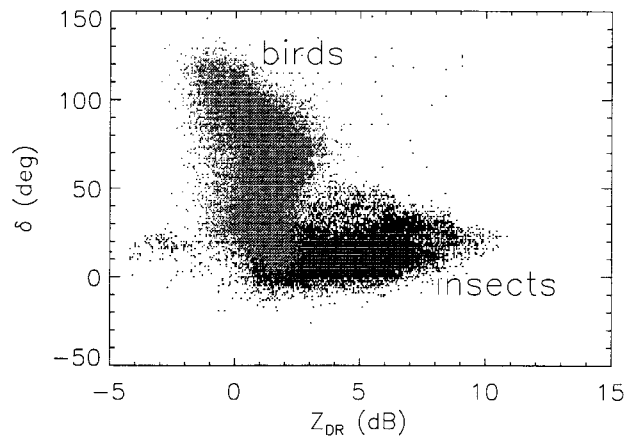


FIG. 12. The  $Z_{DR}$ - $\delta$  scattergrams for insects and birds. Data for insects were collected on 10 August 1993 in the morning hours. The bird data were collected on 7 October 1996, at night.

imum of the cross section for horizontal polarization in the tail look. The global maxima of  $Z_{DR}$  are slightly offset from the side to the head view. Birds' sizes are well into the resonance regime which explains the  $Z_{DR}$  and  $\delta$  patterns. In contrast to insects,  $\delta$  changes significantly with azimuth (about  $100^\circ$ , Fig. 13c). Such striking azimuthal pattern of  $\delta$  is a characteristic tell-tale signature of passerines.

The correlation coefficient is lower than about 0.75 and also has the same axial symmetry as  $Z_{DR}$  or  $K_{DP}$  (Fig. 13d).

##### 2) CHAFF AND GROUND CLUTTER

Because chaff needles have high conductivity, are very elongated, and are horizontally oriented, they would induce larger  $Z_{DR}$  and  $K_{DP}$  values than precipitation with the same reflectivity factor. This conjecture needs to be experimentally verified. Measurements have been made in chaff that demonstrate significant circular depolarization, which allows mapping of entrained chaff into a precipitation region (Moninger and Kropfli 1987).

Ground clutter, including that caused by anomalous propagation, has distinct polarimetric characteristics. On average, its  $Z_{DR}$  is zero,  $\delta$  is uniformly distributed in the  $360^\circ$  interval, and the  $\rho_{hv}$  is smaller than 0.7.

## 5. Summary and conclusions

A heuristic overview of weather radar polarimetry and its possible applications to surveillance radars has been presented. Polarization has in its favor the infor-

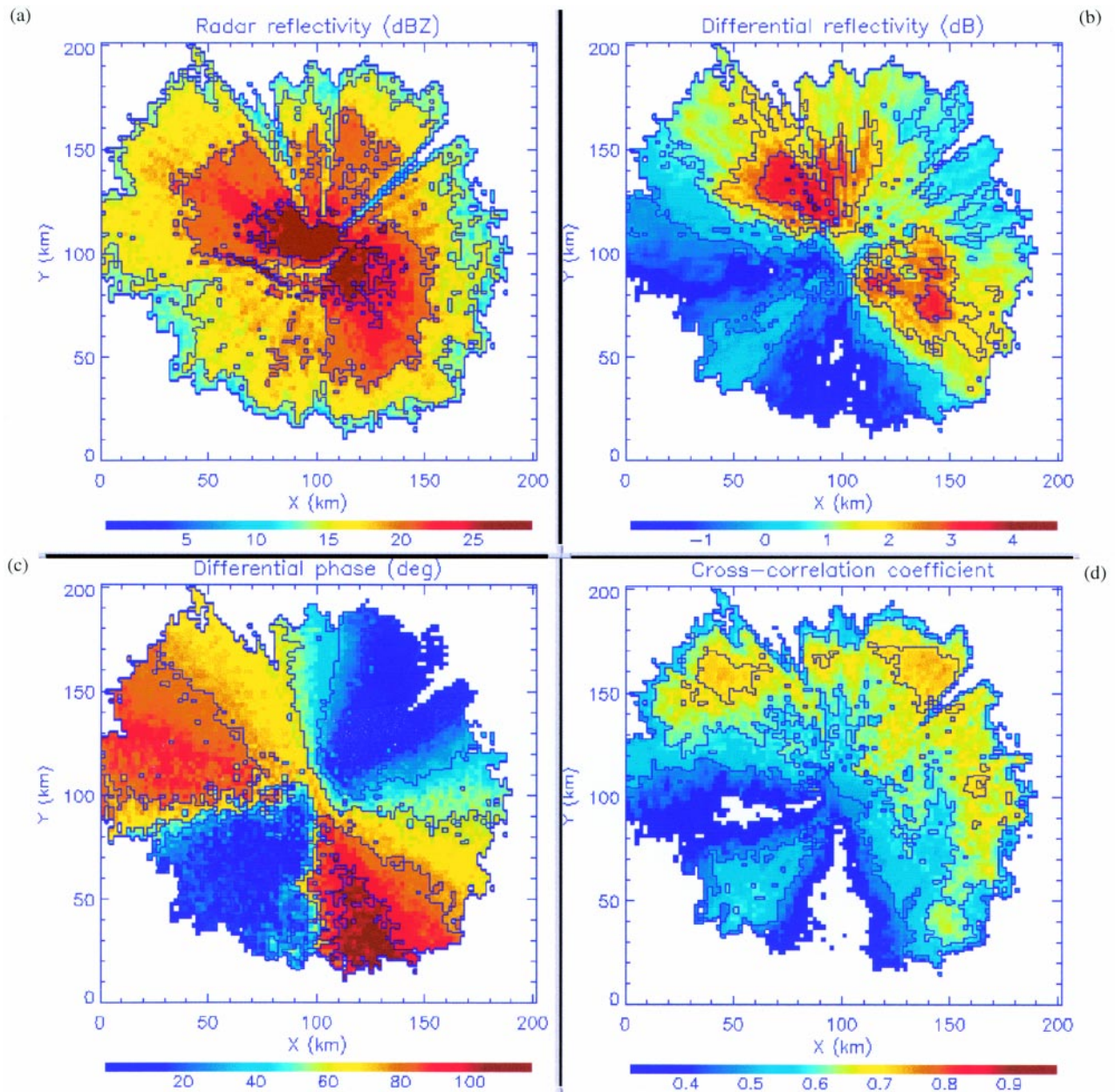


FIG. 13. Fields of (a) reflectivity factor (dBZ), (b) differential reflectivity (dB), (c) differential phase (deg), and (d) correlation coefficient from migrating songbirds (passerines). The elevation angle is  $0.5^\circ$ , the date is 13 August 1997, and the time is 0236 UTC.

mation that it reveals about precipitation types and amounts. This has been amply demonstrated by the examples of polarimetric fields. Better rainfall measurements, identification of hail regions, and isolation of rain amounts in the mixture with hail are possible in rain and hailstorms. Definite mapping of the rain-snow boundary has been demonstrated and might lead to a better quantitative estimation of precipitation in winter storms. Relatively simple automatic procedures to map the polarimetric radar data into precipitation

types are feasible, and a result from one has been illustrated. It is argued that such classification is a necessary step in the path to better determination of precipitation amounts. Another intriguing prospect is to monitor charge buildup and subsequent discharge in electrically active storms. It was shown that clear separation of bird returns from insect returns can be made in the differential reflectivity and backscatter differential phase data. These benefits come with a price, namely, a threefold increase in data amounts that does

require sophisticated processing. But as modern computing and display capabilities outrace existing methodologies, it is inevitable that polarization will find its way into operational weather radars.

*Acknowledgments.* The authors are indebted to the NSSL technical and engineering staff that have developed and continue to maintain the Cimarron polarimetric radar. J. Carter and D. Sirmans installed the microwave components, and A. Zahrai integrated the remote control and signal processing functions. M. Schmidt and R. Wahkinney were responsible for calibration and maintenance. The T-28 operation was supported by the National Science Foundation Division of Atmospheric Sciences lower atmospheric research facilities deployment pool. Dr. J. Straka, from the University of Oklahoma, was instrumental in securing participation of the T-28 aircraft and in developing versions of the classification algorithm. Anonymous reviewers have improved the paper with their constructive criticisms.

## References

Atlas, D., S. Y. Matrosov, A. J. Heymsfield, M. D., Chou, and D. B. Wolff, 1995: Radar and radiation properties of ice clouds. *J. Appl. Meteor.*, **34**, 2329–2345.

Aydin, K., and V. Giridhar, 1992: C-band dual-polarization radar observables in rain. *J. Atmos. Oceanic Technol.*, **9**, 383–390.

—, T. A. Seliga, and V. Balaji, 1986: Remote sensing of hail with a dual linear polarization radar. *J. Climate Appl. Meteor.*, **25**, 1475–1484.

—, V. N. Bringi, and L. Liu, 1995: Rain-rate estimation in the presence of hail using S-band specific differential phase and other radar parameters. *J. Appl. Meteor.*, **34**, 404–410.

Balakrishnan, N., and D. S. Zrnica, 1990: Estimation of rain and hail rates in mixed-phase precipitation. *J. Atmos. Sci.*, **47**, 565–583.

Battan, L. J., 1973: *Radar Observations of the Atmosphere*. University of Chicago Press, 324 pp.

Bringi, V. N., and A. Hendry, 1990: Technology of polarization diversity radars for meteorology. *Radar in Meteorology*, D. Atlas, Ed., Amer. Meteor. Soc., 153–190.

—, T. A. Seliga, and K. Aydin, 1984: Hail detection with a differential reflectivity radar. *Science*, **225**, 1145–1147.

Caylor, I. J., and V. Chandrasekar, 1996: Time-varying ice crystal orientation in thunderstorms observed with multiparameter radar. *IEEE Trans. Geosci. Remote Sens.*, **34**, 847–858.

Doviak, R. J., and D. S. Zrnica, 1993: *Doppler Radar and Weather Observations*. Academic Press, 562 pp.

Hendry, A., and G. C. McCormick, 1976: Radar observation of the alignment of precipitation particles by electrostatic fields in thunderstorms. *J. Geophys. Res.*, **81**, 5353–5357.

Herzogh, P. H., and A. R. Jameson, 1992: Observing precipitation through dual-polarization radar measurements. *Bull. Amer. Meteor. Soc.*, **73**, 1365–1374.

Jameson, A. R., 1983: Microphysical interpretation of multiparameter radar measurements in rain. Part I: Interpretation of polarization measurements and estimation of raindrop shapes. *J. Atmos. Sci.*, **40**, 1792–1802.

—, 1991: A comparison of microwave techniques for measuring rainfall. *J. Appl. Meteor.*, **30**, 32–54.

Krehbiel, P., T. Chen, S. McCrary, W. Rison, G. Gray, and M. Brook, 1996: The use of dual channel circular-polarization radar observations for remotely sensing storm electrification. *Meteor. Atmos. Phys.*, **59**, 65–82.

Meischner, P., C. Collier, A. Illingworth, J. Joss, and W. Randeu, 1997: Advanced weather radar systems in Europe: The COST 75 action. *Bull. Amer. Meteor. Soc.*, **78**, 1411–1430.

Mendel, J., 1995: Fuzzy logic systems for engineering: A tutorial. *Proc. IEEE*, **83**, 345–377.

Metcalf, J. I., 1993: Observation of the effects of charging electric fields on the orientation of hydrometeors in a thunderstorm. *Bull. Amer. Meteor. Soc.*, **74**, 1080–1083.

—, 1997: Temporal and spatial variations of hydrometeor orientations in thunderstorms. *J. Appl. Meteor.*, **36**, 315–321.

Moninger, W. R., and R. A. Kropfli, 1987: A technique to measure entrainment in cloud by dual-polarization radar and chaff. *J. Atmos. Oceanic Technol.*, **4**, 75–83.

Mueller, E. G., and R. P. Larkin, 1985: Insects observed using dual-polarization radar. *J. Atmos. Oceanic Technol.*, **2**, 49–54.

Ryzhkov, A., and D. S. Zrnica, 1995a: Precipitation and attenuation measurements at a 10-cm wavelength. *J. Appl. Meteor.*, **34**, 2121–2134.

—, and —, 1995b: Comparison of dual-polarization radar estimators of rain. *J. Atmos. Oceanic Technol.*, **12**, 249–256.

—, and —, 1996: Assessment of rainfall measurement that uses specific differential phase. *J. Appl. Meteor.*, **35**, 2080–2090.

—, and —, 1998: Discrimination between rain and snow with a polarimetric radar. *J. Appl. Meteor.*, **37**, 1228–1240.

—, V. B. Zhuravlyov, and N. A. Rybakova, 1994: Preliminary results of X-band radar studies of clouds and precipitation. *J. Atmos. Oceanic Technol.*, **11**, 133–139.

—, D. S. Zrnica, and B. A. Gordon, 1998: Polarimetric method for ice water content determination. *J. Appl. Meteor.*, **37**, 125–134.

Sachidananda, M., and D. S. Zrnica, 1986: Differential propagation phase shift and rainfall rate estimation. *Radio Sci.*, **21**, 235–247.

—, and —, 1987: Rain rate estimated from differential polarization measurements. *J. Atmos. Oceanic Technol.*, **4**, 588–598.

Seliga, T. A., and V. N. Bringi, 1976: Potential use of radar differential reflectivity measurements at orthogonal polarizations for measuring precipitation. *J. Appl. Meteor.*, **15**, 69–76.

—, K. Aydin, and H. Direskeneli, 1986: Disdrometer measurements during an intense rainfall event in central Illinois: Implications for differential reflectivity radar observations. *J. Climate Appl. Meteor.*, **25**, 835–846.

Stewart, R., 1992: Precipitation types in the transition region of winter storms. *Bull. Amer. Meteor. Soc.*, **73**, 287–296.

Straka, M. J., 1996: Hydrometeor fields in a supercell storm as deduced from dual-polarization radar. Preprints, *18th Conf. on Severe Local Storms*, San Francisco, CA, Amer. Meteor. Soc. 551–554.

—, and D. S. Zrnica, 1993: An algorithm to deduce hydrometeor types and contents from multiparameter radar data. Preprints, *26th Conf. on Radar Meteorology*, Norman, OK, Amer. Meteor. Soc., 513–515.

Vivekanandan, J., V. N. Bringi, M. Hagen, and P. Meischner, 1994: Polarimetric radar studies of atmospheric ice particles. *IEEE Trans. Geosci. Remote Sens.*, **32**, 1–10.

- Znic, D. S., and N. Balakrishnan, 1990: Dependence of reflectivity factor—rainfall relationship on polarization. *J. Atmos. Oceanic Technol.*, **7**, 792–795.
- , and A. Ryzhkov, 1996: Advantages of rain measurements using specific differential phase. *J. Atmos. Oceanic Technol.*, **13**, 454–464.
- , and ———, 1998: Observation of insects and birds with a polarimetric radar. *IEEE Trans. Geosci. Remote Sens.*, **36**, 661–668.
- , W. D. Rust, and W. L. Taylor, 1982: Doppler radar echoes of lightning and precipitation at vertical incidence. *J. Geophys. Res.*, **87**, 7179–7191.

